Dynamic tuft cell expansion during gastric metaplasia and dysplasia

B Jang, H Kim *et al*. *J Pathol Clin Res* https://doi.org/10.1002/cjp2.352

Supplementary Figures S1–S14

Supplementary Tables S1–S3

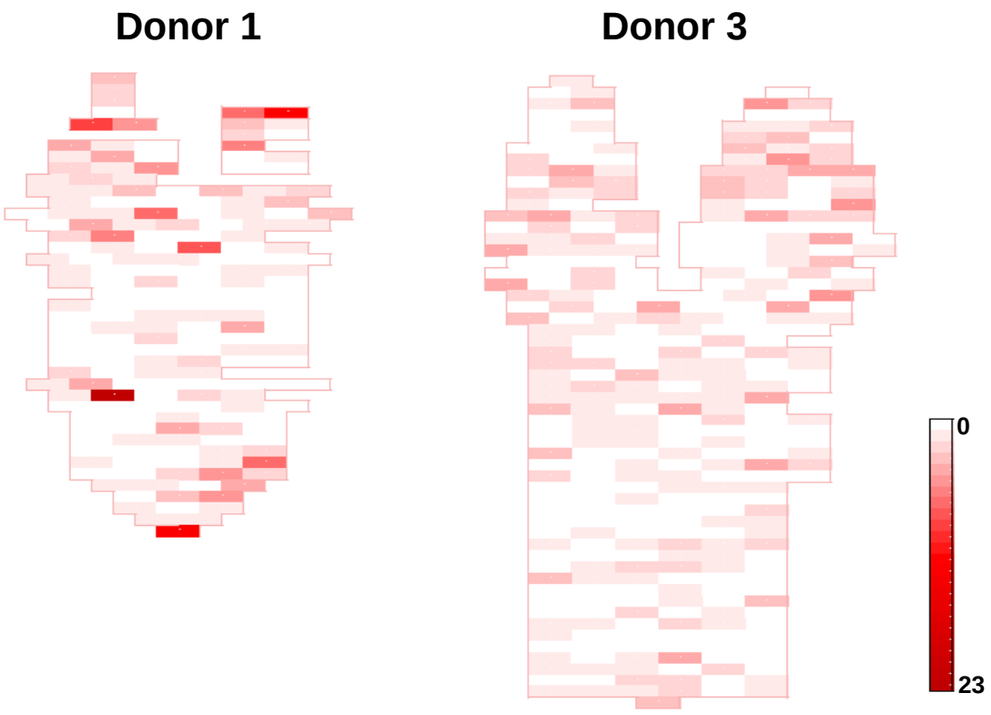

Figure S1. Distribution of tuft cells in the normal stomach of human donors. Two-dimensional maps of the numbers of POU2F3-positive cells in tissue microarrays covering the entire stomach of two donors (Donor1 and Donor 3).

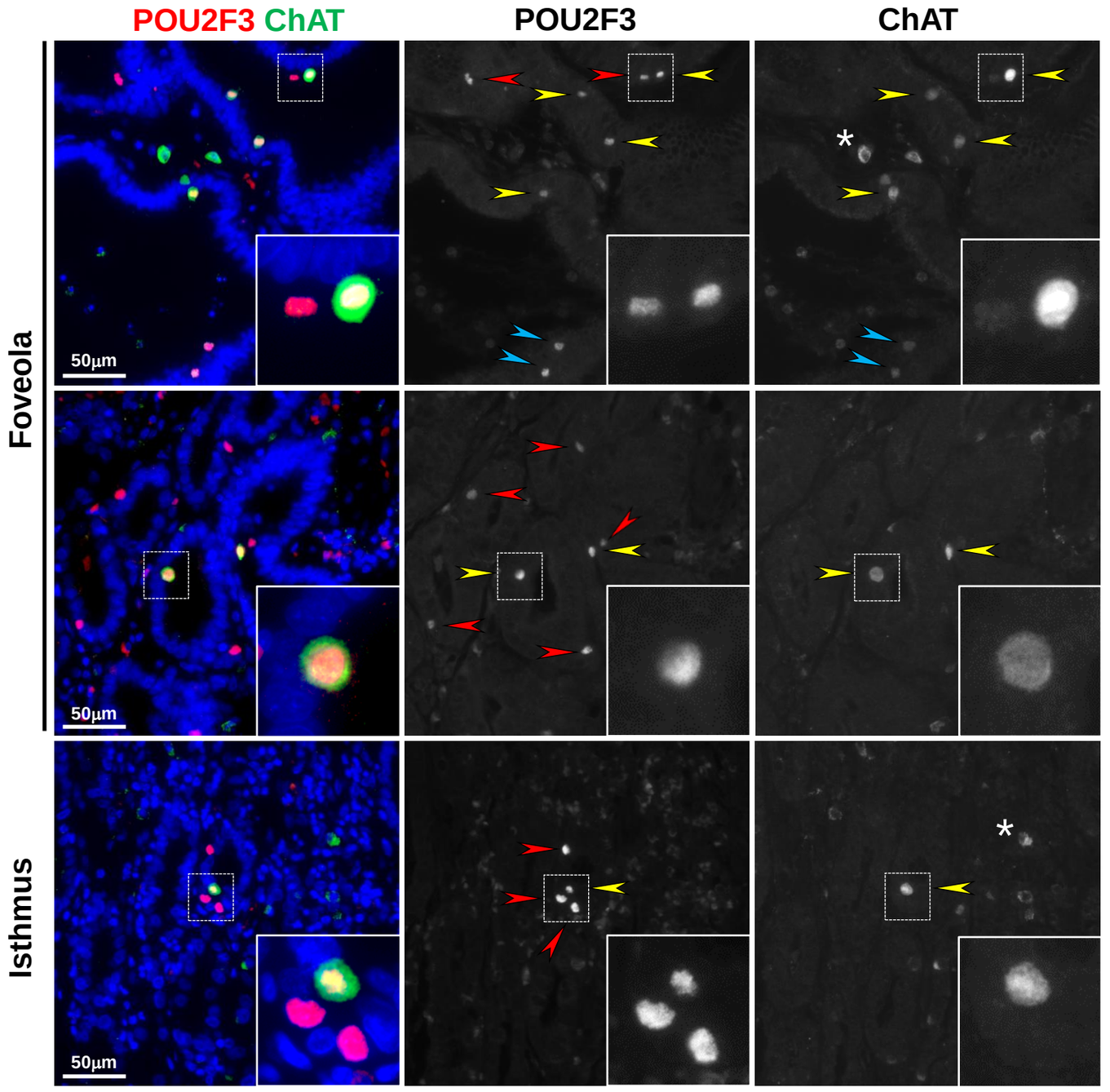

Figure S2. Tuft cell hyperplasia in the stomach of Ménétrier's disease. Co-immunostaining for POU2F3 and Choline acetyltransferase (ChAT) in the hyperplastic foveolar epithelium. POU2F3 single-positive cells (red arrow heads) are more frequently observed than POU2F3 and ChAT double-positive cells (yellow arrow heads). Blue arrow heads indicate POU2F3 positive cells with an weak ChAT expression. White asterisks indicate ChAT single-positive cells in the subepithelial stroma.

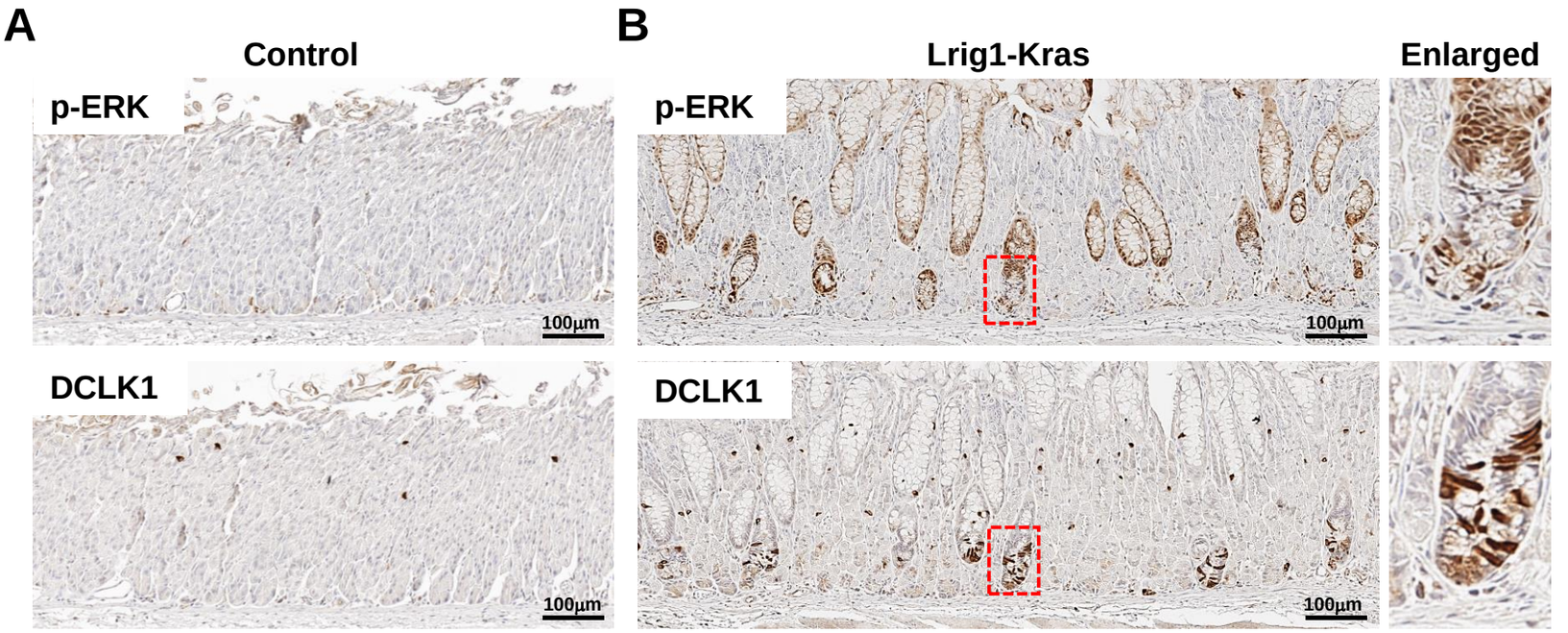

Figure S3. Tuft cell expansion confined to the hyperplastic glands induced by Kras activation. Immunostaining was performed for DCLK1 and phospho-ERK (p-ERK) in serial sections of the stomachs of control and *Lrig1-Kras* mice. (**A**) In control mice, there was no expression of p-ERK, and DCLK1-positive tuft cells were rare. (**B**) In contrast, Lrig1-Kras mice exhibited foveolar hyperplasia with strong p-ERK expression, and tuft cell hyperplasia was exceptionally observed in p-ERK-positive glands.

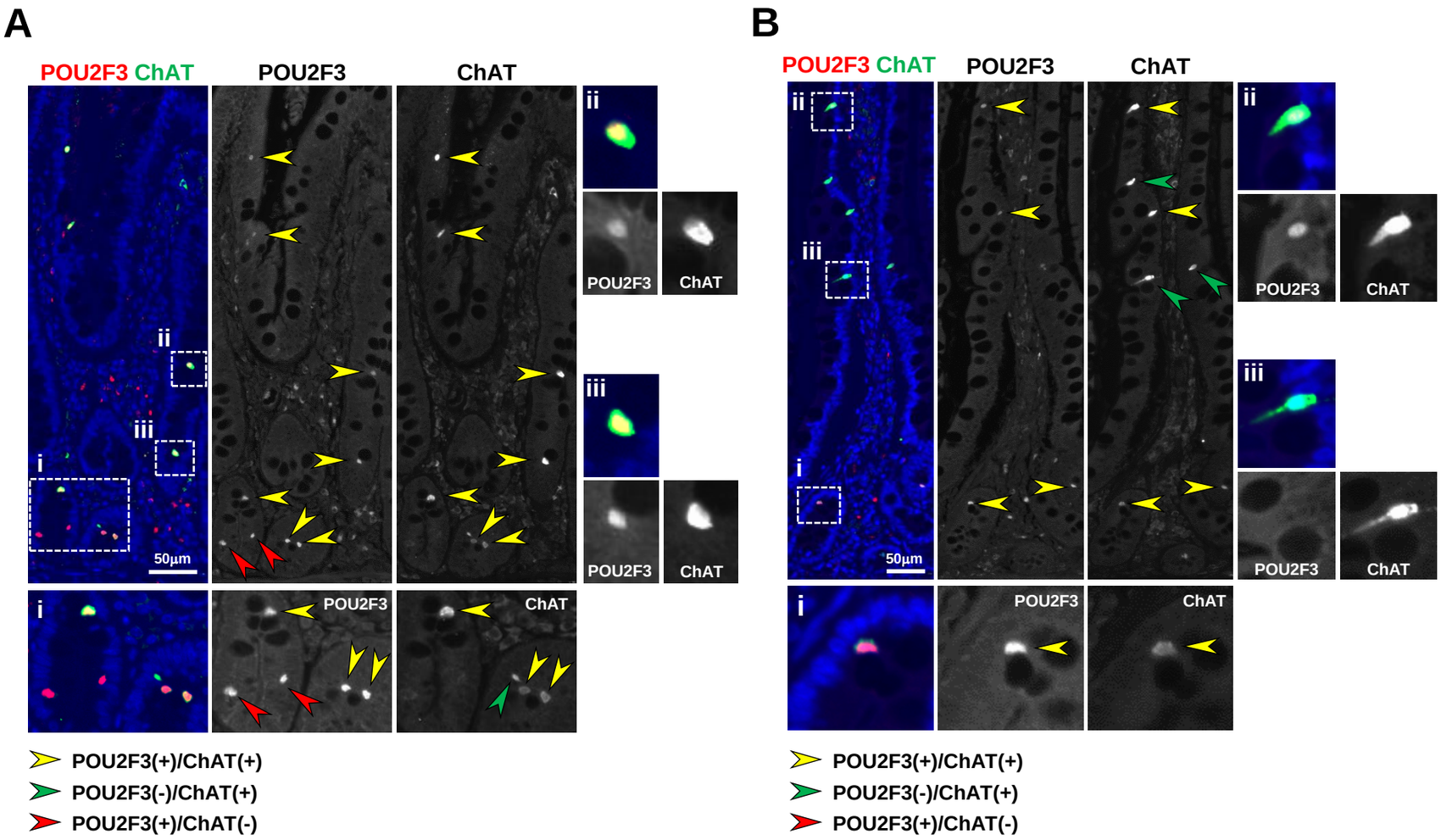

Figure S4. Tuft cells in the crypts and villi of normal small intestine. (**A, B**) Co-immunostaining for POU2F3 and Choline acetyltransferase (ChAT) in normal small intestine. Yellow arrow heads in (A) and (B) indicate POU2F3 and ChAT double-positive cells. POU2F3 single-positive cells (indicated by red arrow heads) are only seen at the crypts (A), whereas elongated tuft cells with a strong ChAT expression (indicated by yellow arrow heads) are mostly observed in the villi (B).

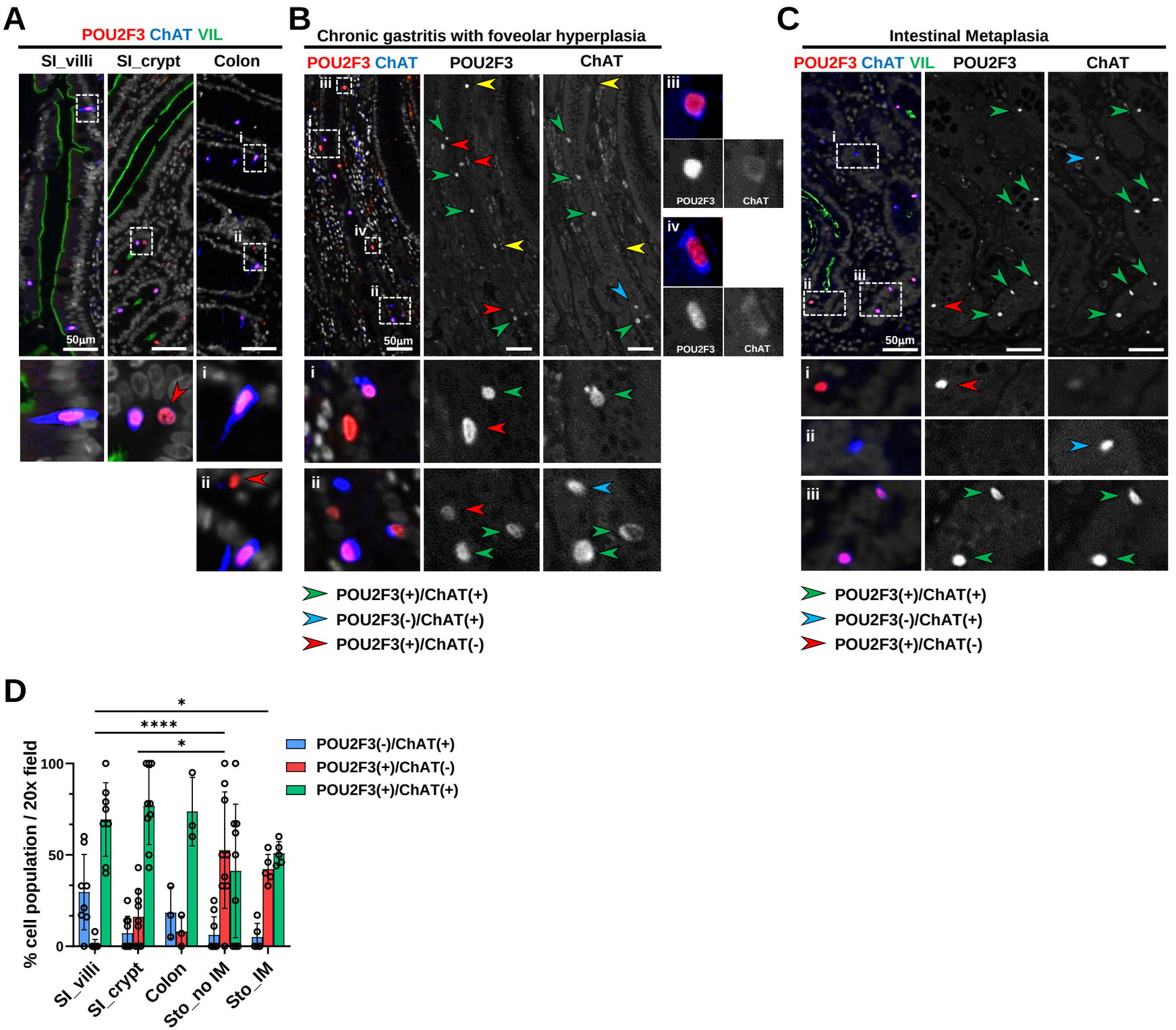

Figure S5. Characteristics of newly emerged tuft cells in chronic gastritis and intestinal metaplasia of human stomach. (**A**) Co-immunostaining for POU2F3, Choline acetyltransferase (ChAT), and Villin (VIL) in normal small intestine (SI) and colon. (**B**) Co-immunostaining for POU2F3 and ChAT in the gastric mucosa with foveolar hyperplasia. (**C**) Co-immunostaining for POU2F3, ChAT, and VIL in intestinal metaplasia (IM). Green arrow heads in (B) and (C) denote POU2F3 and ChAT double-positive cells, while blue arrow heads denote ChAT single-positive cells and red arrow heads denote POU2F3 single-positive cells. Yellow arrow heads indicate POU2F3-positive cells with an weak ChAT expression. Dotted boxes in (A, B, C) indicate enlarged areas. (**D**) Proportions of cells per 20X field according to POU2F3 and ChAT positivity in SI, colon, and gastric mucosa with or without IM. Mean ± SD. One-way ANOVA with Tukey's multiple comparisons test. *$p < 0.05$, **$p < 0.01$, ***$p < 0.001$, ***$p < 0.0001$.

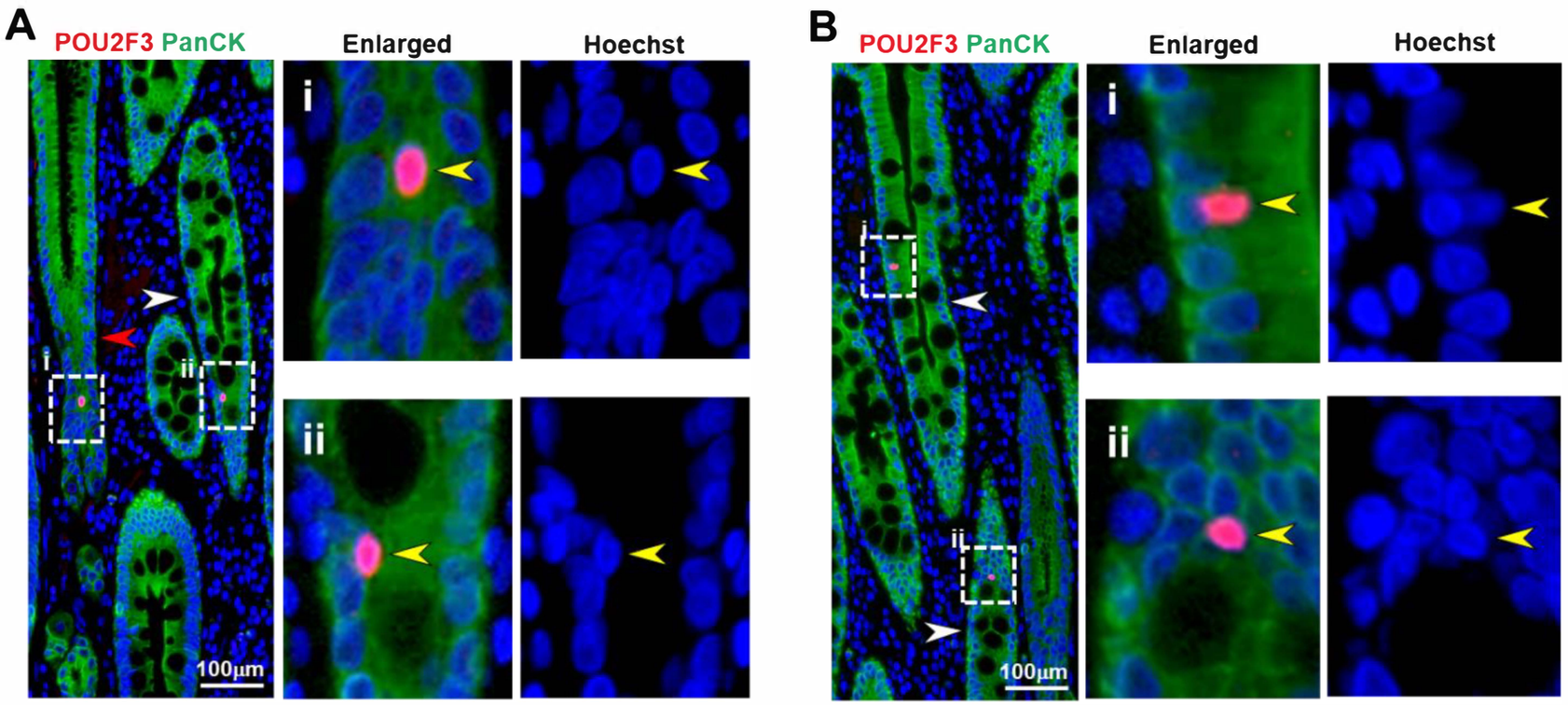

Figure S6. Tuft cells in intestinal metaplasia. (**A, B**) Co-immunostaining for POU2F3 and pan-cytokeratin (panCK), an epithelial marker, in intestinal metaplasia. White dotted boxes denote POU2F3-positive cells co-expressing panCK (indicated by yellow arrow heads in A and B) in foveolar epithelium (indicated by red arrowhead in A) and metaplastic epithelium (indicated by white arrowheads in A and B).

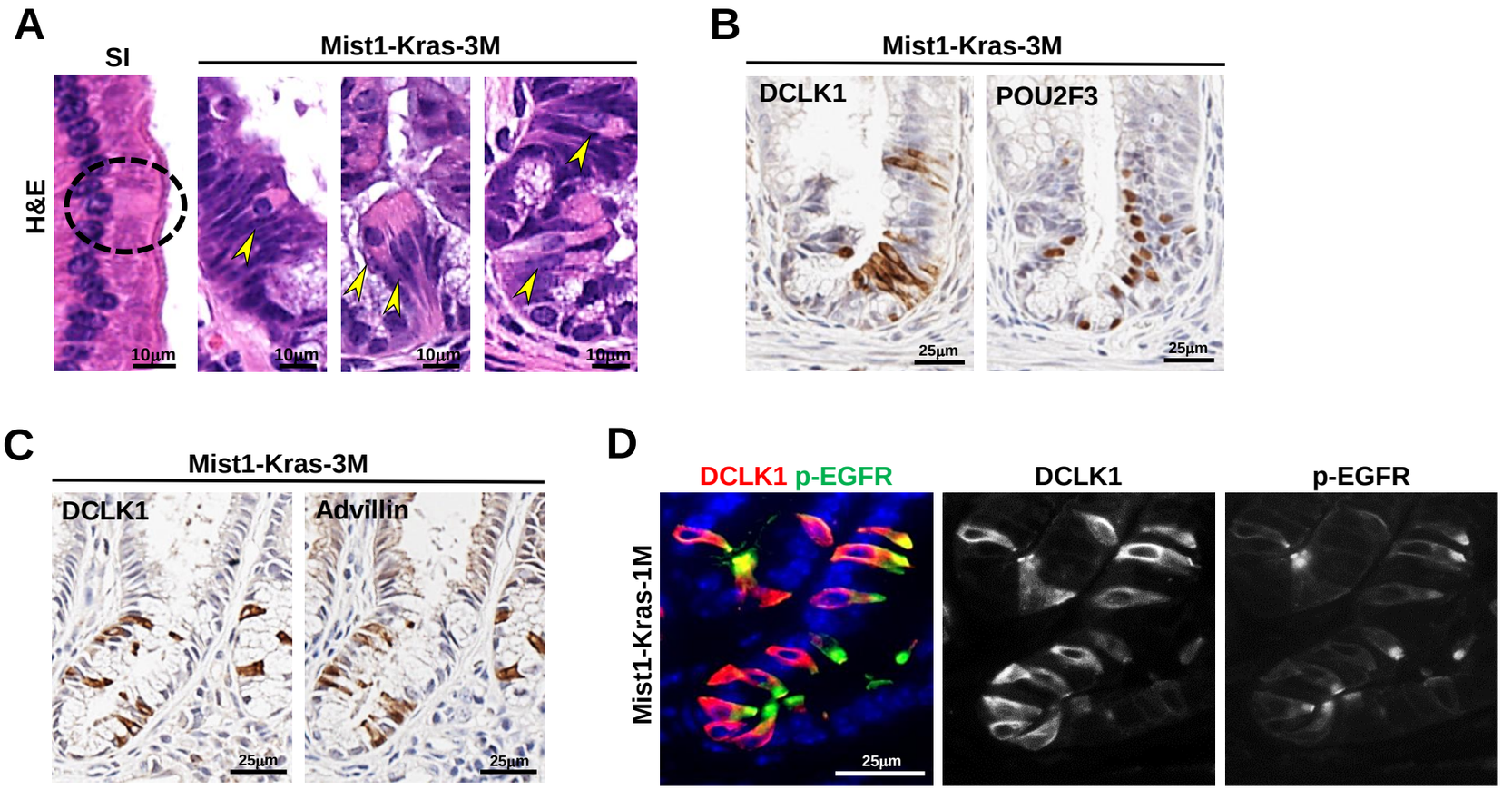

Figure S7. Expression of tuft cell markers in DCLK1-positive cells in Mist1-Kras mice. (**A**) H&E images of tuft cells in the small intestine (SI) (indicated by dotted circle) and Mist1-Kras mice at 3 months (3M) after induction (indicated by yellow arrow heads). (**B, C**) Immunostaining for DCLK1 and POU2F3 (B) or Advillin (C) in serial sections of Mist1-Kras mice. (**D**) Co-immunostaining for DCLK1 and phospho-EGFR (p-EGFR) in the stomach of Mist1-Kras mice at one month (1M) after induction.

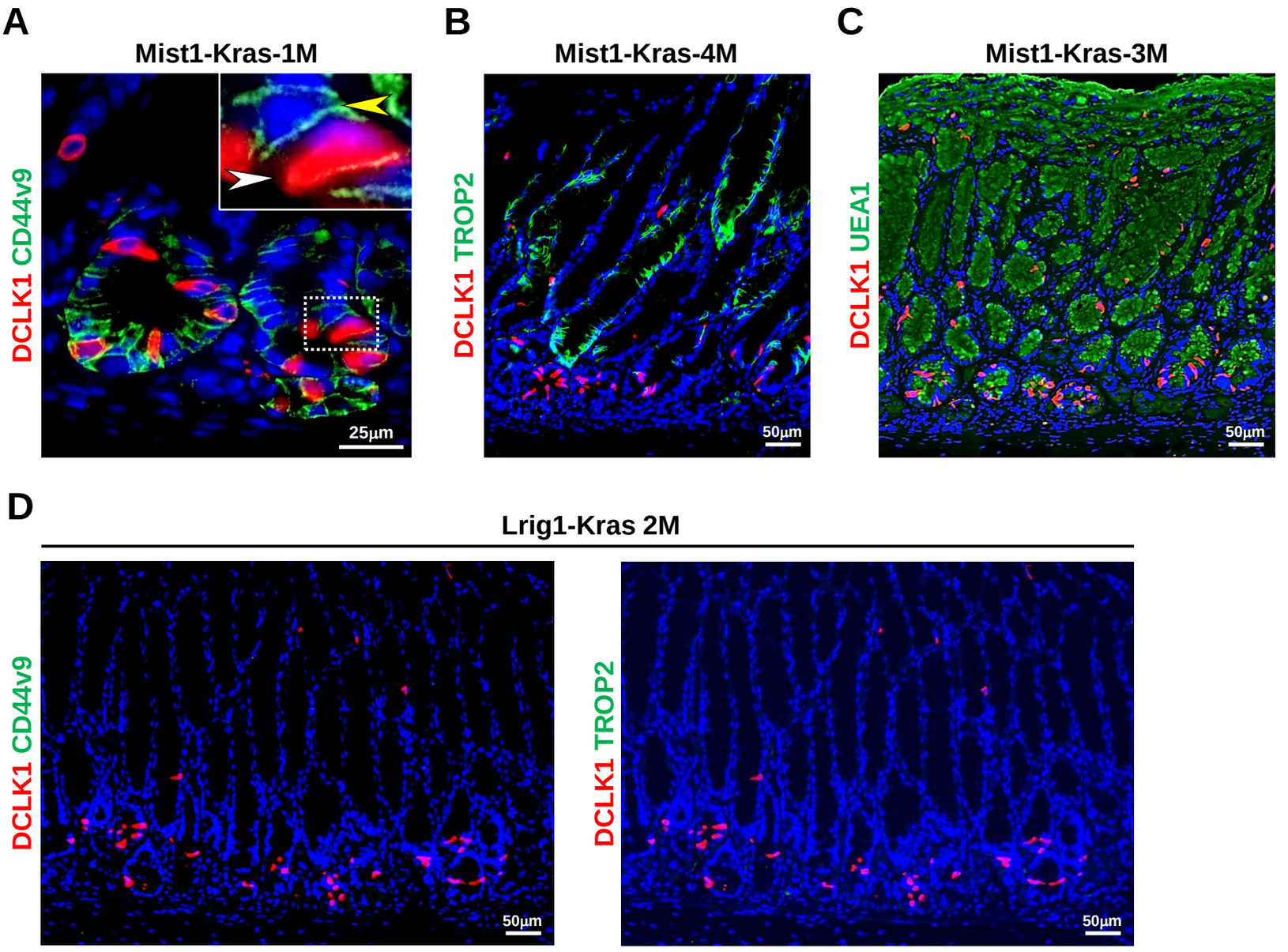

Figure S8. Associations of tuft cells with metaplastic and dysplastic markers (**A**) Co-immunostaining for DCLK1 and CD44v9 in Mist1-Kras mice at 1 month (1M). White dotted box indicates enlarged inlet area. Yellow arrow head indicates a CD44v9-positive metaplastic cell, while white arrow head indicates DCLK1-positive tuft cell. (**B**) Co-immunostaining for DCLK1 and TROP2 in Mist1-Kras mice at 4 months (4M). (**C**) Co-immunostaining for DCLK1 and UEA1 at 3 months (3M). (**D**) Co-immunostaining for DCLK1 and CD44v9 or TROP2 in Lrig1-Kras mice at 2 months (2M).

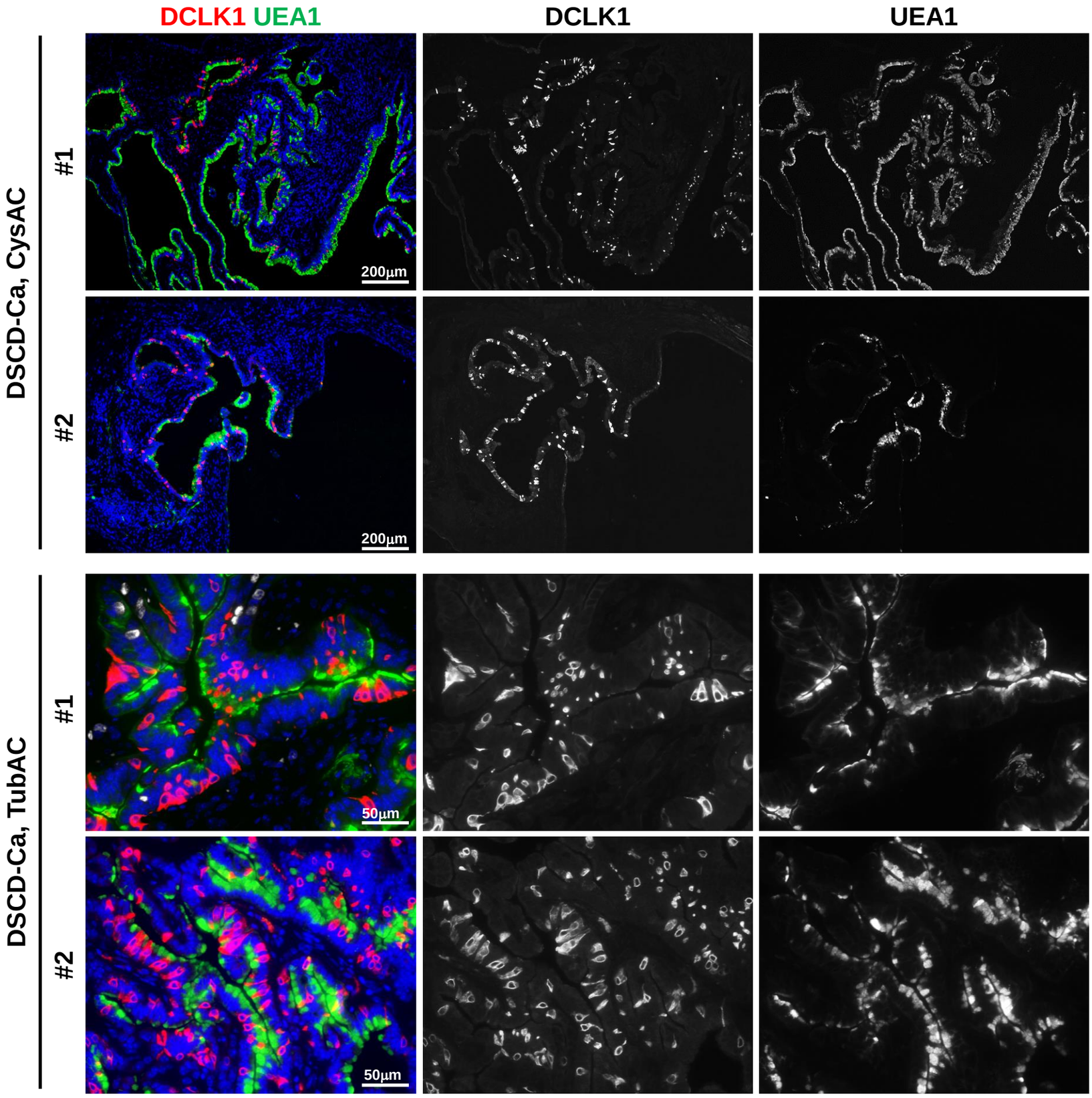

Figure S9. Enrichment of Tuft cells in mucin-rich tumor glands in dysplastic stem cell-derived cancers (DSCD-Ca). Representative images of co-immunostaining for DCLK1 and UEA1 in the cystic (CysAC) or tubular (TubAC) adenocarcinomas formed at 10-13 weeks after implanting CD133/CD166 double-positive DSCs from Meta4 organoids in the nude mice (n=8). Numerous tuft cells are seen in the glands with abundant mucin producing cells.

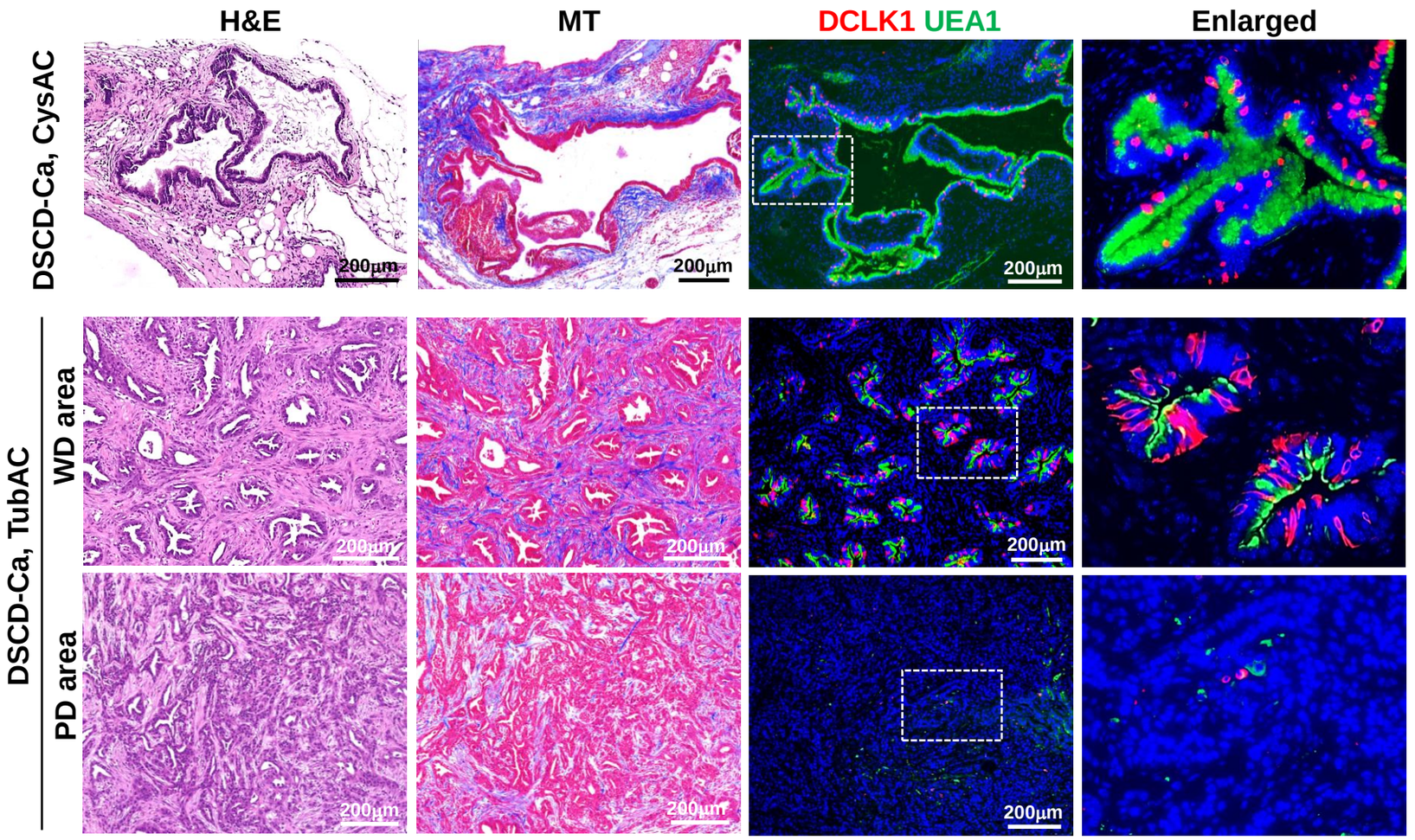

Figure S10. Histologic characteristics of microenvironment for tuft cell population in dysplastic stem cell-derived cancers (DSCD-Ca). Representative images of H&E, Masson-Trichrome (MT) staining and co-immunostaining for DCLK1 and UEA1 in the cystic (CysAC) or tubular (TubAC) adenocarcinoma formed at 13 weeks after implanting CD133/CD166 double-positive stem cells from Meta4 organoids in the nude mice (n=8). Numerous tuft cells are observed in the cystic or large tubular glands surrounded by abundant fibrotic stroma, but they are extremely rare in the poorly-differentiated areas

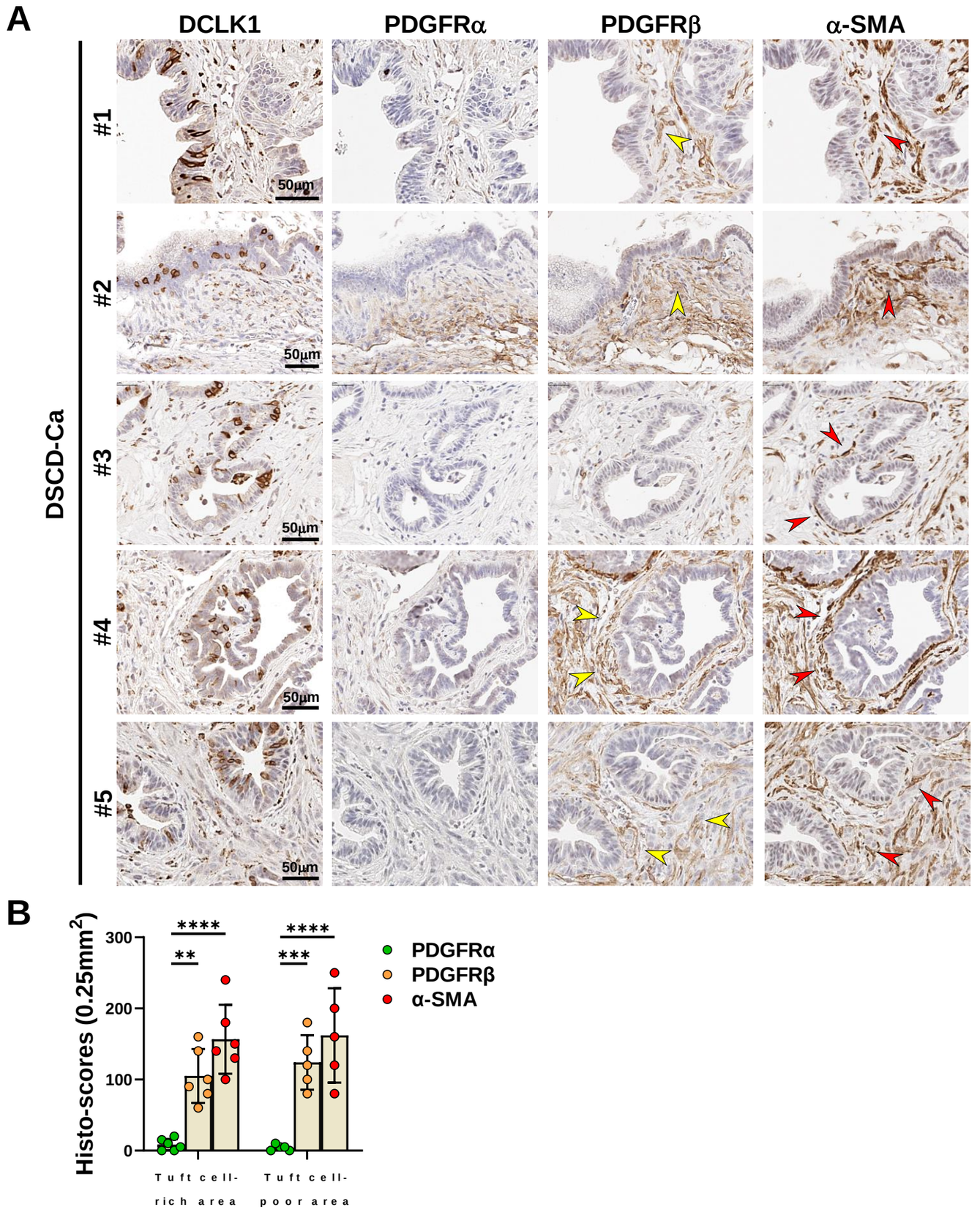

Figure S11. Expression of fibroblast markers around tuft cell-rich tumor glands dysplastic stem cell-derived cancers (DSCD-Ca). (**A**) Representative images of immunostaining for Dclk1, PDGFRα, PDFGRβ, and α-smooth muscle actin (SMA) in the tuft cell-rich cancer glands generated by implanting CD133/CD166 double-positive stem cells from Meta4 organoids (12 to 13 weeks) in nude mice (n=6). Fibroblasts located nearby tuft cells tend to be positive for PDGFRβ (black arrow heads) and α-SMA (yellow arrow heads), but negative for PDGFRα. (**B**) Histo-scores of fibroblast markers in tuft cell-rich (n=6) or tuft cell-poor areas (n=5). Mean±SD. One-way ANOVA with Tukey's multiple comparisons test. **p<0.01, ***p<0.001, ****p<0.0001.

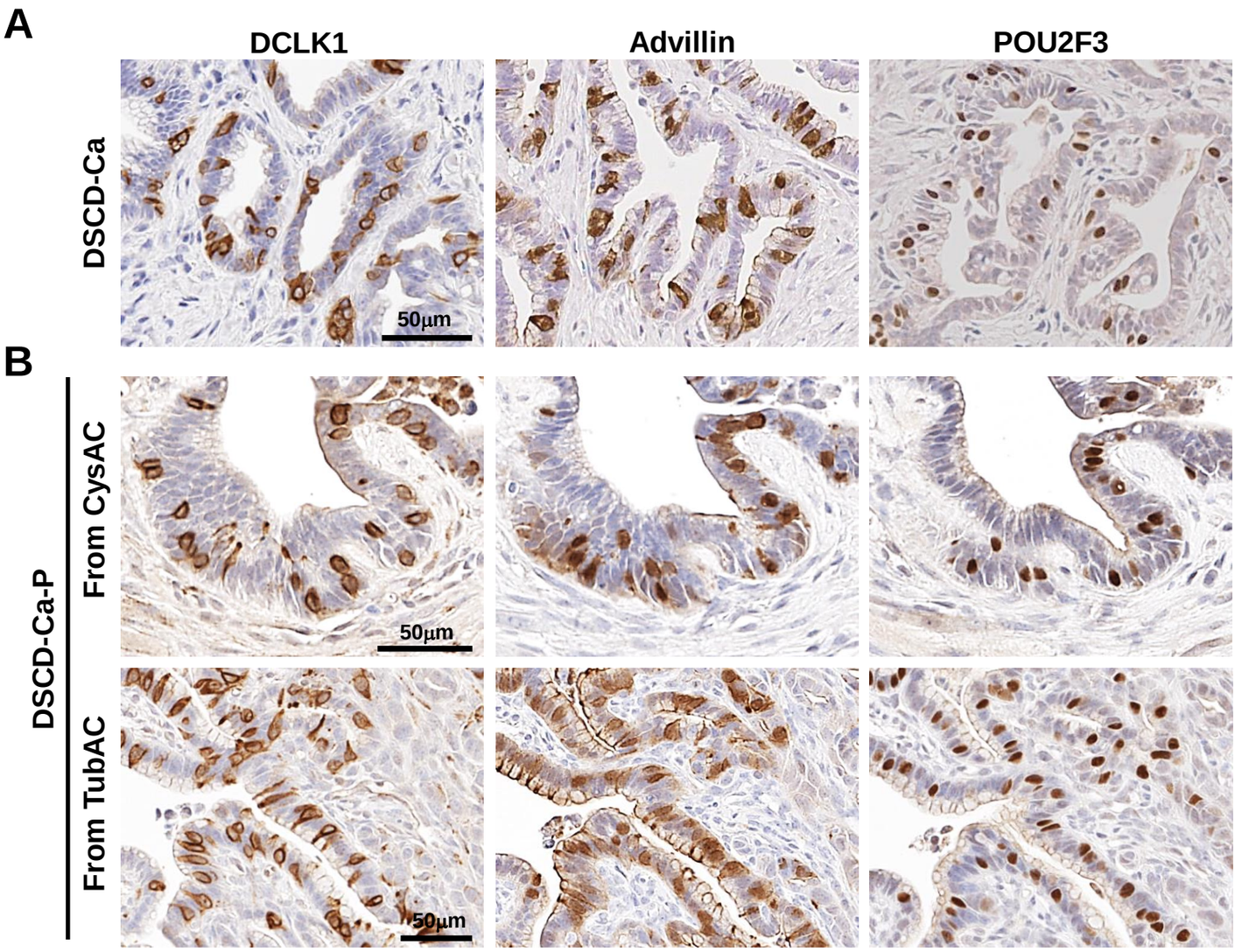

Figure S12. Tuft cell markers' expression in dysplastic stem cell-derived cancers (DSCD-Ca in nude mice. (**A**, **B**) Representative images of immunostaining for DCLK1, Advillin and POU2F3 in the DSCD-Ca (13 weeks) (A) or passaged DSCD-Ca (DSCD-Ca-P, 3 weeks) generated by re-inoculating either cystic (CysAC) or tubular (TubAC) adenocarcinomas (B) in nude mice. DCLK1-positive cells consistently express Advillin and POU2F3.

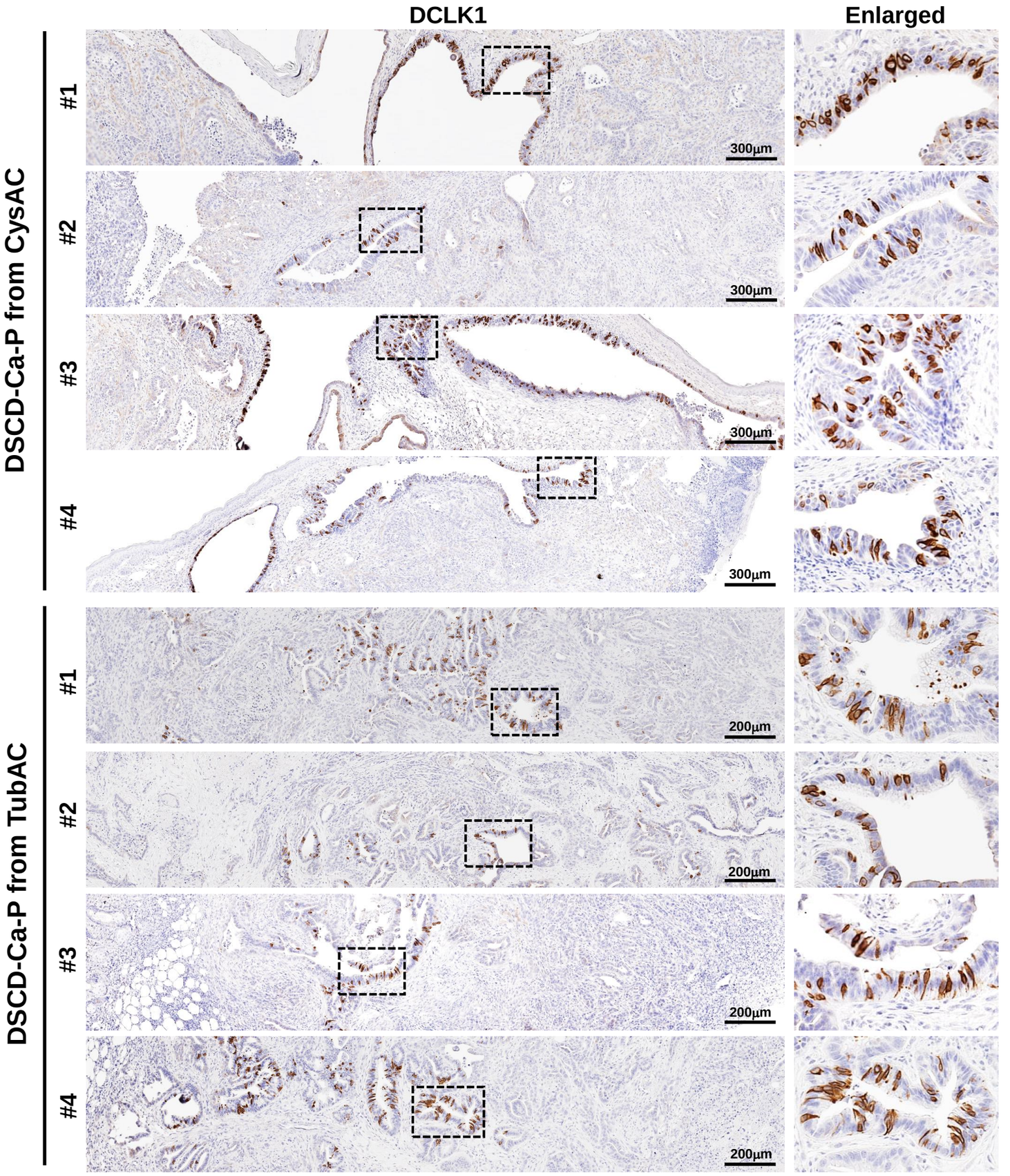

Figure S13. Representative images of immunostaining for DCLK1 in passaged dysplastic stem cell-derived cancers (DSCD-Ca-P) formed at 3 or 7 weeks after re-inoculating cystic (CysAC, n=4) or tubular (TubAC, n=4) adenocarcinoma cells in nude mice. Tuft cells are concentrated in the areas exhibiting cystic or large tubular structures, while they are scarcely observed in the invasive regions. The dotted boxes depict enlarged areas.

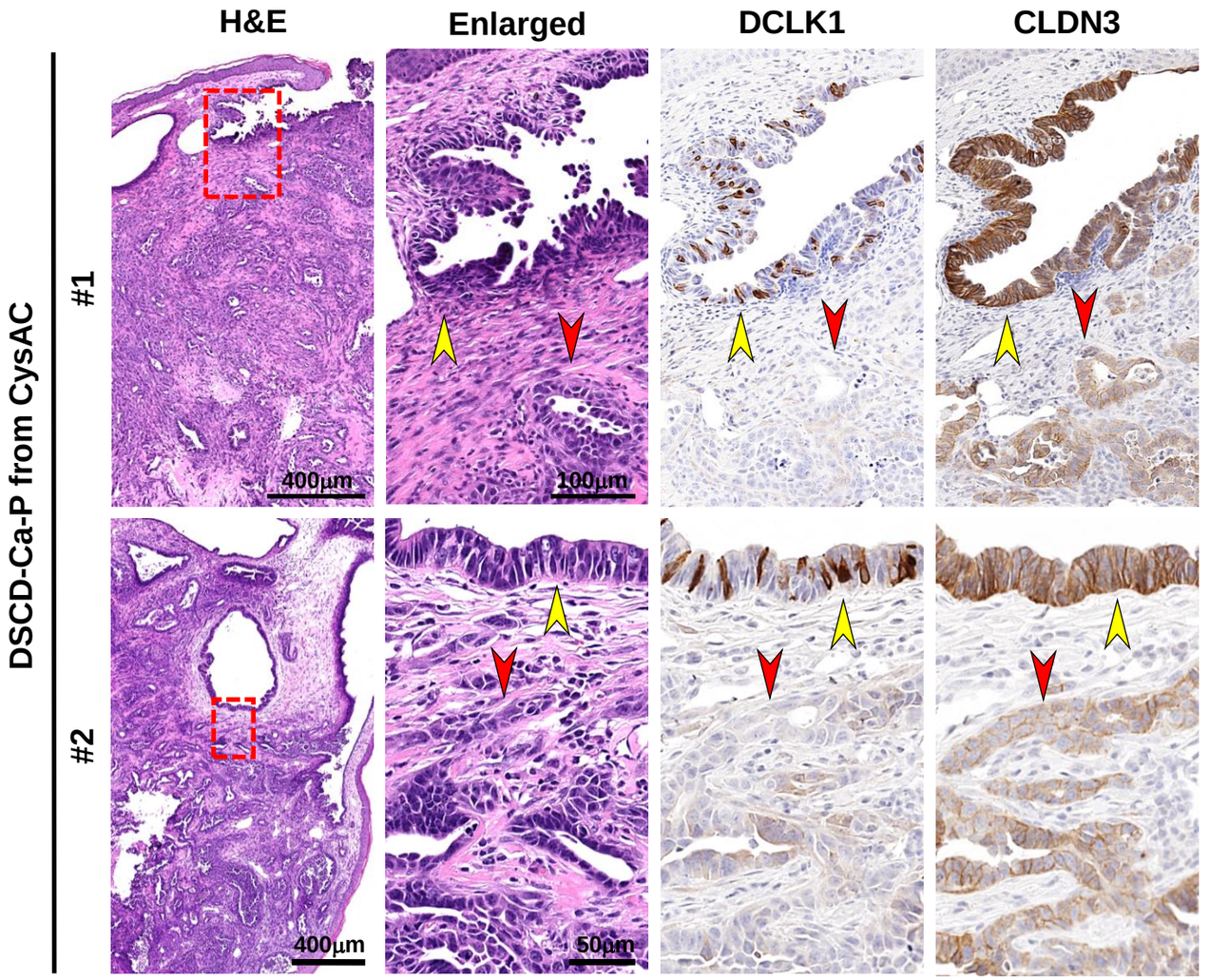

Figure S14. Representative images of H&E and immunostaining for DCLK1 or Claudin-3 (CLDN3) in passaged dysplastic stem cell-derived cancers (DSDC-Ca-P) formed at 7 weeks after re-inoculating cystic adenocarcinoma (CysAC) cells in nude mice. Tuft cells are exclusively observed in the cystic areas exhibiting a strong CLDN3 expression (yellow arrow heads), but no tuft cells are present in the adjacent invasive area with a lower level of CLDN3 (red arrow heads). The red dotted boxes depict enlarged area.

Table S1. Characteristics of human stomach donors

Donor	AGE	Gender	WEIGHT (lb)	HEIGHT (in)	BMI	Status
1	57	Female	140	61	26.4	Overweight
2	52	Male	197	70	28.3	Overweight
3	21	Male	176	76	21.4	Normal

Body mass index (BMI) was calculated with the formula of weight (lb)/[height (in)]^{2}x703.

Table S2. Characteristics of gastric tumor patients

		TA	GC
Case no.		12	156
Age, Mean ± SD		72±9	68±13
Gender (%)	Male	10 (83)	90 (58)
	Female	2 (17)	66 (42)
Location (%)	Body	2 (17)	
	Antrum	10 (83)	
EGC/AGC (%)	EGC		100 (64)
	AGC		56 (36)
Histology (%)	WD		7 (4)
	MD		39 (25)
	PD		63 (40)
	PCC (SRCC)		36 (23)
	Others		11 (8)
TNM stage (%)	I		78 (50)
	II		33 (21)
	III		45 (29)
	IV		0 (0)

TA, tubular adenoma; GC, gastric cancer; SD, standard deviation;
EGC, early gastric cancer; AGC, advanced gastric cancer; WD, well differentiated; MD, mode rately differentiated; PD, poorly differentiated; PCC, poorly cohesive carcinoma; SRCC, signe t ring cell carcinoma; TNM, tumor-lymph node-metastasis.

Table S3. List of primary antibodies for immunostaining

Antibody	Species	Vender, Catalog#	Dilution
Acetylated Tubulin	Mouse	Sigma, T6793	1:500
Advillin	Rabbit	Novus Bio, NBP2-34118	1:1,000
CD44v9	Rat	Cosmo Bio, LKG-M001	1:15,000
Choline Acetyltransferase	Goat	Millipore, AB144P	1:1,000
Chromogranin A	Rabbit	ImmunoStar, 20085	1:1,000
CLDN3	Rabbit	ABclonal, A2946	1: 1,000
DCLK1	Rabbit	Sigma-Aldrich, HPA065008	1:1,000
Alexa Fluor® 647 Anti-EGFR (phospho Y1068)	Rabbit	Abcam, ab205828	1:500
ERK	Rabbit	Cell Signaling, 4695	1:3,000
phospho-ERK	Rabbit	Cell Signaling, 4370	1:3,000
H/K ATPase	Mouse	Fitzgerald,10R-H100b	1:10,000
Ki-67 for mouse	Rat	BioLegend, 652402	1:500
Ki-67 for mouse/human	Rabbit	Abcam, ab16667	1:500
P120	Mouse	BD Biosciences, 610133	1:100
PDGFRα	Rabbit	Cell Signaling, 3164S	1:200
PDGFRβ	Rabbit	Thermo Fisher, MA5-15143	1:200
POU2F3	Rabbit	Sigma, HPA019652	1:2,000
α-SMA	Mouse	Sigma,A5228	1:500
STAT6	Rabbit	Cell Signaling, 53975	1:1,000
Phospho-STAT6	Rabbit	Cell Signaling, 565545	1:1,000
TFF3	Rabbit	Gift from Daniel K. Podolsky	1:1,000
TROP2	Goat	R&D Systems, AF1122	1:500
Fluorescein conjugated- anti-UEA1		Vector, FL-1061	1: 2,000
Villin	Mouse	Santa Cruz, sc-58897	1:000